Chemistry–A European Journal
Research Article
doi.org/10.1002/chem.202103775
Chemistry Europe
European Chemical Societies Publishing
www.chemeurj.org

Revisiting the Fundamental Nature of Metal-Ligand Bonding: An Impartial and Automated Fitting Procedure for Angular Overlap Model Parameters

Moritz Buchhorn,[a] Robert J. Deeth,[b] and Vera Krewald*[a]

Abstract: The properties and reactivities of transition metal complexes are often discussed in terms of Ligand Field Theory (LFT), and with *ab initio* LFT a direct connection to quantum chemical wavefunctions was recently established. The Angular Overlap Model (AOM) is a widely used, ligand-specific parameterization scheme of the ligand field splitting that has, however, been restricted by the availability and resolution of experimental data. Using *ab initio* LFT, we present here a generalised, symmetry-independent and automated fitting procedure for AOM parameters that is even applicable to formally underdetermined or experimentally inaccessible systems. This method allows quantitative evaluations of assumptions commonly made in AOM applications, for example, transferability or the relative magnitudes of AOM parameters, and the response of the ligand field to structural or electronic changes. A two-dimensional spectrochemical series of tetrahedral halido metalates ($[M^{II}X_4]^{2-}$, M = Mn–Cu) served as a case study. A previously unknown linear relationship between the halide ligands' chemical hardness and their AOM parameters was found. The impartial and automated procedure for identifying AOM parameters introduced here can be used to systematically improve our understanding of ligand–metal interactions in coordination complexes.

Introduction

Transition metal compounds are relevant in many areas of chemistry; they serve as catalysts, pigments, photosensitisers, and drugs to name a few. They show an immense variance in their properties, reactivities and stabilities, which is rooted in the malleability of their electronic structures. Many examples in the literature have shown that the interplay of synthesis, spectroscopy and theory is essential for the targeted electronic structure design of transition metal complexes with improved properties.[1–6] An early and well-known example is the electronic structure analysis of vanadyl in terms of a molecular orbital picture.[7] This interplay rests on chemical concepts, which are often derived from quantum mechanics or accurate measurements, but are commonly applied and used in an intuitive manner. With quantum chemistry being able to predict electronic structures and thus contributing to explain experimental observations,[3,8–12] detailed connections to established chemical concepts can be made to quantitatively evaluate their scope and limitations.

Ligand Field Theory (LFT) is one of the most successful models in chemistry: by connecting readily available information on structure, symmetry and chemical building blocks, it can predict spectroscopic and magnetic properties of a vast array of transition metal complexes.[13–15] LFT evaluates the effect of ligands, or more specifically of the electrostatic field created by the ligands, on the d or f electrons of a central metal. When ligands are considered as point charges in a purely ionic picture of bonding, Crystal Field Theory (CFT) emerges as an extreme scenario within LFT.[13,16] While CFT can be deduced from fundamental principles and therefore considered *ab initio*, the representation of ligands as point charges or point dipoles is a poor approximation to real electron distributions and CFT gives d orbital splittings which are in quantitatively poor agreement with experiment.[17]

LFT has been interpreted differently by various authors.[18–23] It can be considered as a parameterization scheme that is intended to capture the interaction of the metal d orbitals with the ligands empirically. Ideally, these empirical parameters can be interpreted chemically. Which kind of parameterization is used depends on the complex considered. For example, the ligand-field splitting parameter Δ is valid for homoleptic cubic octahedral and tetrahedral complexes, but becomes ill-defined for other geometries. Many parameterizations are global, which means they apply to a whole complex and cannot be transferred to another. The utility of such a global scheme lies in the fact that the respective parameters such as ligand field stabilization energy, interelectronic repulsion, etc. can be meaningfully compared between complexes. However, global

[a] M. Buchhorn, Prof. Dr. V. Krewald
TU Darmstadt, Department of Chemistry, Theoretical Chemistry, Alarich-Weiss-Straße 4, 64287 Darmstadt (Germany)
E-mail: krewald@chemie.tu-darmstadt.de
[b] Prof. Dr. R. J. Deeth
University of Warwick, Department of Chemistry, University of Warwick, Gibbet Hill, Coventry, CV4 7AL (United Kingdom)

Supporting information for this article is available on the WWW under https://doi.org/10.1002/chem.202103775

Part of the Chemistry Europe joint Special Collection on Quantum Bioinorganic Chemistry.

schemes are not intended to capture the impact of single M–L bonds, so they do not allow for an interpretation in terms of functional groups.

The Angular Overlap Model (AOM) is a parameterization scheme within LFT, which was developed by Schäffer and Jørgensen.[24] An appealing characteristic of the AOM is the description of metal-ligand interactions in terms of local parameters. The complex is divided into spatial regions that are centered around the metal-ligand bonds and are characterized in terms of σ and π interactions between metal and ligand.[20,25] The fundamental idea is to consider the field imposed by the ligands on the metal d orbital energies as a perturbation and thus fit parameters for the individual metal-ligand interaction to the d orbital energy differences.[26] Besides the intuitive chemical interpretation, the definition and quantification of individual interactions may in principle permit a transfer of the corresponding parameters to other complexes with the same metal-ligand bond.[27] While the AOM parameterization is well established for ionic metal-ligand interactions, an often quoted limitation is its failure for systems with strong differential orbital covalency, which has been defined as the difference in the metal d character in different types of d orbital.[25,28] We note here that in the puristic ligand field model, the d orbitals remain pure and therefore the concept of differential orbital covalency cannot be included in this model.[13,29,30] However, other interpretations of covalency in the ligand field and AOM context have been given.[31–33] As discussed in more detail below, large non-spherical contributions to the ligand field matrix are outside the remit of the AOM model.[13]

Historically and today, AOM parameter fitting procedures make use of experimental data sensitive to the valence orbitals of predominant d or f orbital character, e.g. UV-vis spectra or magnetic data.[34–38] Although it has in principle always been within the scope of the AOM to describe complexes with arbitrary or no symmetry, this was almost impossible to achieve, mainly because experimental data provides limited information. For instance, data on optical transitions in transition metal complexes are generally limited to at most four d orbital energy differences. This limits the number of fittable parameters dramatically, and very often resulted in assumptions about the AOM parameters. These assumptions or constraints were usually not generally applicable and hence not transferrable to related complexes. In some cases, assumptions were made to reduce complexity, e.g. neglecting π-interactions for ammine ligands[20] or imposing constraints such as $e_\sigma \approx 4e_\pi$.[39,40] In other cases, an additional parameter was introduced to account for the otherwise inexplicable positioning of a d orbital energy level. The most prominent example for this is the low energy of the d_{z^2} orbital in square planar $[CuCl_4]^{2-}$. The attempts to explain and parameterize this observation eventually divided the AOM formalism into two models: the AOM and a branch called Cellular Ligand Field (CLF) model.[41,42] The introduction of coordination voids was criticised,[18] although recent work by one of us (R.J.D.) has sought to rejustify the void cell concept.[43,44] For the parameterization scheme utilized in this work, the models are identical.

Even with the predictive power that single- and multi-determinantal quantum chemistry methods have now reached, LFT and the AOM have not become obsolete.[45–49] Quite in contrast, the implementation of *ab initio* LFT (aiLFT)[31,50,51] has been a significant success that illustrates the need for straightforward chemical interpretations of complex quantum chemical data.[32,52–55] The aiLFT approach can be understood as a way of translating the multidimensional information of a CASSCF or CASSCF/NEVPT2 wavefunction into concepts that are readily understood by experimental and theoretical chemists.[31,50,51,56] Naturally, such a compression of information comes at a certain cost; in this instance it is the model Hamiltonian that recovers only a specific part of the full complexity of the much more general *ab initio* wavefunction and energies. It cannot be used, for example, to treat charge transfer transitions which would require explicit inclusion of the ligand orbitals.[50] This simplification is desired, however, since aiLFT's focus on the metal-ligand interactions means that they can be described in terms of chemically intuitive σ and π interactions. The loss of generality is the price to pay for a simple and understandable model.

The aiLFT analysis delivers the ligand field matrix. However, a standardized and impartial way for obtaining AOM parameters from a quantum chemical calculation of an arbitrary coordination complex is not yet available. In this work, we introduce such an automated fitting procedure for AOM parameters derived from aiLFT. We employ systematic asymmetric distortions of the ligand sphere to obtain a large number of independent matrix elements and thereby overcome the limitations imposed on fits to experimental data. Importantly, the approach proposed in this work differs from AOM parameter fitting procedures employed previously in that it does not rely on symmetry considerations or experimental data. The procedure introduced here can be applied to a variety of complexes as long as the requirements for the underlying aiLFT analysis are met, i.e. a reasonable representation of the electronic structure with an active space containing only the metal d or f orbitals. Naturally, this excludes complexes with non-innocent ligands.[57,58] Our concept and its success are illustrated with tetrahedral metal halides that form a two-dimensional spectrochemical series. Additionally, a linear relationship between Pearson's chemical hardness[59,60] and the AOM parameters is found. This previously unknown relationship connects the AOM parameters with a measurable chemical quantity and may provide further avenues for the classification and interpretation of quantum chemical calculations of transition metal complexes and their ligand fields.

Methodology

The ligand field potential

Ab initio ligand field theory, developed and implemented in ORCA,[61] makes a direct connection between ligand field theory and the electronic energies computed with complete active space self consistent field (CASSCF) theory, optionally with a

subsequent perturbation theory treatment (NEVPT2). The details of this procedure are presented elsewhere,[31,50,62] so that only a brief summary is given below. The key feature is the construction of an effective ligand field Hamiltonian that acts on a d orbital basis.[50,62] In LFT, this Hamiltonian is derived from experimentally observed d–d transitions, whereas in aiLFT, the respective states are obtained from a CASSCF calculation. The LFT model Hamiltonian consists of a one-electron part, $\hat{V}$, and a two-electron part, $\hat{G}$:

$$\hat{H}_{LF} = \sum_i \hat{V}_{LF}(i) + \sum_{i<j} \hat{G}(i,j) \tag{1}$$

Acting on a d orbital basis, the one-electron operator yields a matrix which is called the *one-electron ligand field matrix* or *ligand field potential* $\mathbf{V}_{LF}$, the elements of which are defined as:

$$v_{ij} = \langle d_i | \hat{V}_{LF} | d_j \rangle \tag{2}$$

In the equation above, the ligand field potential is expressed in terms of a d orbital basis, although one can construct $\hat{H}_{LF}$ (or $\hat{V}_{LF}$, respectively) for an f orbital basis in order to perform a ligand field analysis.[33,38,45] When d orbitals are mentioned in this work, we always refer to the valence d orbitals. $\mathbf{V}_{LF}$ is obtained by a CASSCF calculation with subsequent aiLFT analysis as implemented in the ORCA quantum chemistry package (see Computational Details).

AOM equations

The AOM can be used as a parameterized fitting scheme for the $\mathbf{V}_{LF}$ matrix.[20,41,50] The matrix elements are expressed in terms of the angular overlap factors $F(\theta,\phi,\psi)$, which are determined by the angular positions of the ligands L and the AOM parameters $e_\lambda(r)$:

$$v_{ij} = \sum_L \sum_\lambda F_{L\lambda i} F_{L\lambda j} e_{L\lambda} - \sum_L F_{dsi}\sqrt{e_{Lds}} \cdot \sum_L F_{dsj}\sqrt{e_{Lds}} \tag{3}$$

with $\lambda = \sigma, \pi_x, \pi_y$ and $i,j = 0,1,2,3,4 = xy, yz, z^2, xz, x^2-y^2$. The equations for F can be found in the Supporting Information; a visualization of the interaction including different interaction types is shown schematically in Figure 1. Note that the d–s mixing contribution cannot be included in the first sum, since it is a second order effect and the summations are executed before the multiplication. Deeth and Foulis provided a detailed overview of the d–s mixing formalism.[63]

For ligands without cylindrical symmetry, π_x and π_y interactions must be distinguished. All ligands treated in this work have cylindrical symmetry, so the two interactions are indistinguishable and therefore the labels x and y are dropped in the discussions below. In $F(\theta,\phi,\psi)$, ψ is the rotational angle along the bond axis and can be set to an arbitrary value; we assume ψ to be 0.

Equation 4 shows the 5×5 one-electron ligand field matrix in more detail:

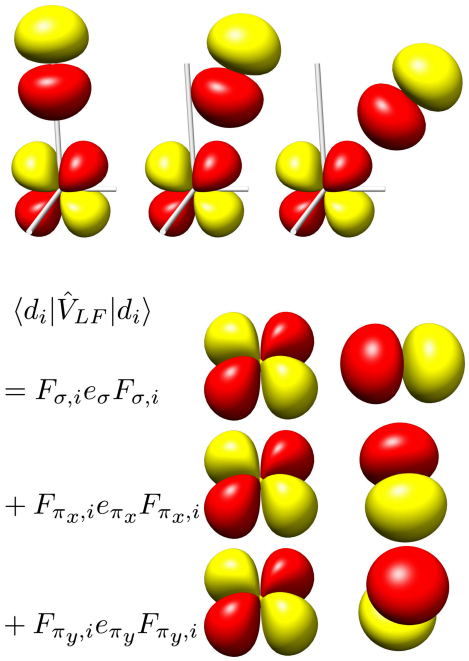

Figure 1. Top: Visualization of the σ-interaction of an arbitrary d orbital with a ligand orbital and its dependency on the polar angle. The square of the angular overlap factor $F^2_{\sigma,i}$ is zero for the left frame, increases in the center and is at its maximum in the right frame. Bottom: Visualization of the interaction between an arbitrary d orbital and ligand orbitals alongside the respective AOM parametrization.

$$\mathbf{H}_{LF} = \mathbf{V}_{LF} + E \cdot \mathbf{1} = \begin{pmatrix} v_{00}+E & v_{01} & v_{02} & v_{03} & v_{04} \\ v_{10} & v_{11}+E & v_{12} & v_{13} & v_{14} \\ v_{20} & v_{21} & v_{22}+E & v_{23} & v_{24} \\ v_{30} & v_{31} & v_{32} & v_{33}+E & v_{34} \\ v_{40} & v_{41} & v_{42} & v_{43} & v_{44}+E \end{pmatrix} \tag{4}$$

$$h_{ij} = \langle d_i | V_{ij} | d_j \rangle + E\delta_{ij} \tag{5}$$

Here, E is the d orbital energy affected by the spherical contribution of the ligand field, ***1*** is the identity matrix. Since $v_{ij} = v_{ji}$ and no complex numbers occur, the ligand field matrix is always hermitian and therefore diagonalizable. When the matrix in equation 4 is diagonalized, the resulting eigenvalues are the perturbed d orbital energies. The eigenvalues represent the increase in energy of the d_i orbital due to ligand field effects. From the symmetric 5x5 matrix $\mathbf{V}_{LF}$, a maximum of 15 independent matrix elements can be fitted. Since one parameter is always the d orbital energy affected by spherical field contributions E, a maximum of 14 AOM parameters can result from the fit. To meet this maximum, a totally asymmetric ligand environment around the central metal is required.

On the parameter *E*

The parameter *E* in equation 4 is rarely mentioned in the AOM literature, because it is irrelevant for the interpretation of the $e_\lambda(r)$ AOM parameters. In the matrix $\mathbf{H}_{LF}$ from aiLFT, the one-electron energy of the d orbitals is included, and hence it also contains the energy which is implicitly assumed to be the ground level in the AOM picture. In previous schemes for obtaining AOM parameters, *E* usually cancelled out and was therefore not easily available for interpretation. Since *E* is explicitly included in the procedure presented here, specifically in the way the equation systems are set up, we want to elaborate on the connection between the AOM equations with and without *E* a little further.

When $\mathbf{H}_{LF}$ as shown in equation 4 is diagonalized, the respective eigenvalues contain $+E$. Since the AOM is only interested in orbital energy differences rather than absolute energies and experimental data can also only yield relative energies, these eigenvalues are subtracted from each other, leaving four equations in which *E* is cancelled out. So while representing the energy of the degenerate $d_{x^2-y^2}$ and d_{z^2} orbitals in octahedral symmetry as $\varepsilon(x^2-y^2)=\varepsilon(z^2)=3e_\sigma$ is not inherently wrong, it implies that *E* will be cancelled out by taking the difference between this and other equations. From a mathematical perspective, there is no justification to say that we could not solve this equation. So the puristic way to write the AOM equations for octahedral symmetry would be:

$$\varepsilon(x^2-y^2)=\varepsilon(z^2)\ =E+3e_\sigma \tag{6}$$

$$\varepsilon(xz)=\varepsilon(yz)=\varepsilon(xy)\ =E+4e_\pi \tag{7}$$

$$\Rightarrow \Delta = 3e_\sigma - 4e_\pi \tag{8}$$

It is immediately clear from these equations that the system is underdetermined and has no single solution. In Figure 2, the classical d orbital energy change due to the ligand field is shown, where the energy levels are labelled as in equation 6 and 7. At this point we want to emphasize that *E* is *not* the d orbital energy of the free ion. In fact, *E* is a function of the M–L bond length and resembles a spherical ligand field potential, while the e_λ parameters represent non-spherical contributions only. As shown below, the response of *E* to variations in the ligand field is easily accessible with the fitting procedure presented here.

Obtaining aiLFT-AOM parameters

Since a generalised black-box procedure for obtaining AOM parameters from the aiLFT analysis was missing, we introduce here how the AOM parameters are calculated starting from an optimized structure of the compound of interest. The next sections refer to Figure 3. The program we developed for fitting the AOM parameters is available upon request.

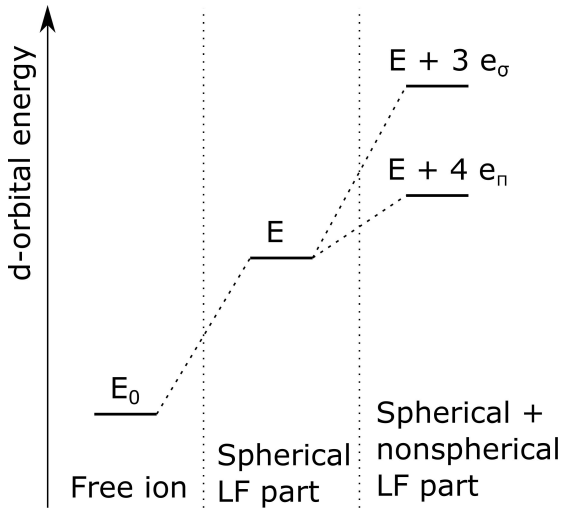

Figure 2. Schematic change of d orbital energies from a free ion to a homoleptic octahedral complex, labelled with the puristic style of AOM equations as in Equations 6 and 7.

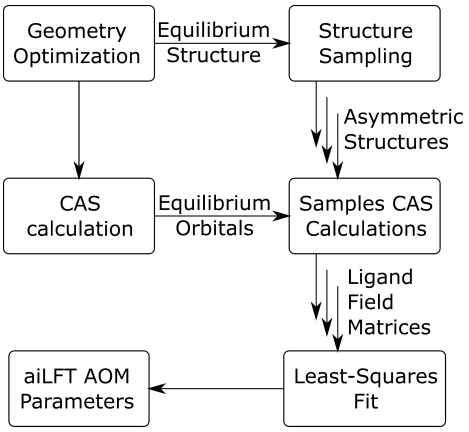

Figure 3. Schematic representation of the AOM fitting procedure.

Asymmetric distortions

The more symmetric a complex is, the fewer independent equations are available in the AOM fitting scheme. In order to avoid underdetermination even in the many highly symmetric complexes, small distortions have to be applied to the structure, while still assuming that the parameters obtained for the minimally distorted molecule are the same as for the initial structure. A similar procedure was already employed by Atanasov et al.[50] and Singh et al.,[31] although the distortions they applied were of a certain symmetry. We set three requirements for the distortions that are applied automatically in our black-box procedure:

1. It should be asymmetric, since high symmetry reduces the number of independent equations.[64,65]
2. It should be small, so it can be safely assumed that the parameters do not change significantly.

3. It should not lead to a geometry in which the electronic structure differs significantly from the equilibrium geometry.

To meet the requirements, we employ a sampling procedure where the M–L bond lengths are varied and at each step a small, arbitrary angular distortion is imposed, thereby satisfying criterion 1. While the bond length variation can be chosen freely, the angle is varied by about 1°, which is sufficient for having more independent matrix elements and small enough to meet requirement 2.

The last requirement is met for every case covered in this work, but not generally. For chelating ligands, the sampling process must ensure that the displacements of the ligating atoms preserve the remainder of the ligand structure, and for bulky ligands the independent displacements must avoid structural clashes. For the small ligands explored in this proof-of-concept work, requirement 3 is well met. The structure sampling step is in the top right corner of Figure 3.

CASSCF calculations

A CASSCF calculation of the equilibrium structure is needed in which the active space consists of the valence d orbitals. Only one successful CASSCF calculation needs to be supplied by the user since the orbital projection feature of ORCA is employed for the subsequent CASSCF calculations on the structures obtained from the sampling process via asymmetric distortions. Compared to the equilibrium geometry, the sampled structures are sufficiently similar to ensure that the projection is successful. In this way, the aiLFT analysis and hence all quantum chemical information for the fitting procedure can be obtained very efficiently. These steps are placed in the center boxes of Figure 3.

Fitting procedure

The actual parameter fit is the bottom part of Figure 3. For every sampled structure, the one-electron ligand field matrix is extracted. Each matrix element corresponds to one equation. The resulting equation system is in general overdetermined and inconsistent, so the solution is approximated via a least-squares fit. The cost of the fit S is subject to minimization and defined as the sum of the squared differences between the found solution and the best solution of each equation. This difference is also called the residue r.[66]

$$S = \sum_i (s_{i,fit} - s_{i,ideal})^2 = \sum_i r_i^2 \tag{9}$$

In general, better results at lower fitting costs are obtained when treating every ligand with its own set of parameters. This may however lead to overparameterizing the problem on a mathematical level. When fitting the parameters, different ligands may therefore be set to share a set of AOM parameters; this is referred to as *grouping*. Exemplifying this with the compounds studied in this work, they have four ligands and d–s mixing is not relevant for the (near) tetrahedral symmetry. With grouped ligands, there are three parameters: E, e_σ and e_π, where E is global and e_σ and e_π are shared by all ligands. When assigning a unique parameter set to each ligand, there are nine parameters: E and four sets of e_σ and e_π parameters. Since up to 15 unique equations are available from V_{LF}, we can perform such an *ungrouped* fit.

Limitations

Ungrouped fitting is not always feasible since V_{LF} is limited to a maximum of 15 equations. When considering complexes with more ligands, distinguishable π_x and π_y interactions and/or a relevant d–s mixing contribution, this limit is easily exceeded. Ligands must then be treated with the same set of parameters, which imposes constraints on the system. Trial calculations show that assigning the same parameter set to several ligands is only successful for perfectly equivalent ligands. Even the small distortions employed in the presented sampling scheme interfere with this requirement because of their totally asymmetric nature.

An inherent problem comes with the underlying equation system, that is the main diagonal elements are clearly defined and have large values, and hence they dominate the fit. They roughly lead to the relationship for Δ and the AOM parameters in a tetrahedral complex. The off-diagonal elements should then help to find the exact minimum on this line, but they have very low numbers and the identified minima can scatter. The behaviour is illustrated in Figure 4, for which ligand grouping was used and the equation system was reformulated in order to reduce the problem to three dimensions. The same concept holds for larger parameter sets, but the ten-dimensional equation system cannot be depicted in human-readable form anymore. More details are given in the Supporting Information.

Computational details

The ORCA 4.2.1 quantum chemistry package[61,67] was used for all calculations except the AOM parameter fitting. Geometries were optimized using the unrestricted Kohn-Sham formalism with the BP86 functional[68,69] and the def2-SVP basis set.[70] The electronic states corresponding to the d orbitals were calculated using the CASSCF procedure[71,72] with the def2-TZVP basis set. The subsequent second-order N-electron valence state perturbation theory (NEVPT2)[73-76] was employed for the calculations in the section "AOM parameters for complexes of the type $[CoX_4]^{2-}$". The active space was chosen to contain the d orbitals and d electrons, which makes up e.g. a CAS(7,5) space in the cobalt complexes considered. The *ab initio* ligand field theory module[50] was then employed to construct the effective ligand field Hamiltonian from the calculated states. The AOM was used to fit the one-electron part of the ligand field Hamiltonian according to our fitting procedure described above.[24,41] For testing purposes, calculations with solvation models and differ-

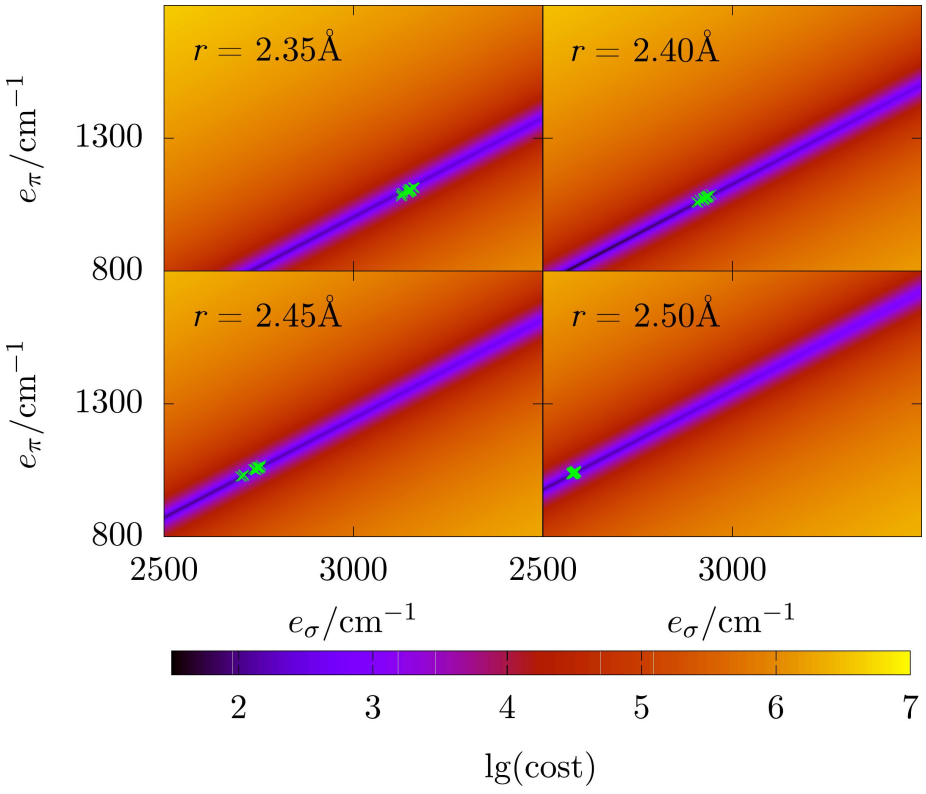

Figure 4. Fitting costs for $[CoCl_4]^{2-}$, calculated with a reduced equation system. Matrix elements on the main diagonal are subtracted from each other in order to cancel out *E*, all chloride ligands are grouped. The plot shows the dependence of the fitting cost *S* (see Equation 9) of a certain parameter set on the two parameters e_σ and e_π . Fitting costs are shown on a logarithmic scale as a colour gradient. Each green point represents the results of an individual fit. The four plots correspond to different M–Cl distances as labelled in the insets.

ent basis sets were run as stated in the main text and Supporting Information.

Results

For this study, (near-)tetrahedral metal halide complexes of the type $[MX_4]^{2-}$ in a two-dimensional spectrochemical series with M = Mn-Cu and X = F-Cl were selected. The series allows two simplifications: the cylindrical symmetry of the halide ligands with respect to the M–L bond implies that the π_x and π_y interactions need not be distinguished, but can be subsumed as a π interaction. Secondly, all complexes considered are of (near) tetrahedral symmetry, therefore no or quite limited d–s mixing is expected and the d–s mixing parameter can be neglected in most cases.

The principles of our automated fitting procedure are demonstrated with $[CoX_4]^{2-}$ complexes, for which ideal tetrahedral coordination environments and no d–s mixing are expected. Experimental data are available for most members of the $[CoX_4]^{2-}$ series. $[CoCl_4]^{2-}$ is readily formed from $CoCl_2$ in hydrochloric acid,[77] can be synthesized in different organic solvents,[78] and crystal structures are well known and spectroscopically investigated.[79,80] For $[CoBr_4]^{2-}$, the ion in solution was not reported, but crystals have been analysed spectroscopically,[80] and the $[CoBr_4]^{2-}$ units were found to be almost tetrahedral.[81,82] The data thin out a little for $[CoI_4]^{2-}$: crystals with almost tetrahedral $[CoI_4]^{2-}$ units are known,[81,83,84] but no electronic spectroscopy data was collected. The only homoleptic anion we must assume to be fictitious is $[CoF_4]^{2-}$. Fluoro complexes of cobalt have been reported with higher cobalt oxidation states of +III and +IV.[85] Publications on the synthesis and characterization of gaseous CoF_3, CoF_4, CoF_4^- and respective cations are known.[86,87]

AOM parameters for complexes of the type $[CoX_4]^{2-}$

In the literature, we can find AOM parameters fitted to experimental data, but they always come with a catch: it is basically impossible to distinguish the split components of the tetrahedral $^4A_2(4F)$, $^4T_2(4F)$, $^4T_1(4F)$ and $^4T_1(4P)$ states.[88] The slight distortions to the tetrahedral units in many crystals are not large enough to affect the spectra significantly. That means even in these distorted environments, there is only one experimental value to fit two parameters on: $\Delta = \frac{4}{3}e_\sigma - \frac{16}{9}e_\pi$. Consequently, it has not been possible to reliably determine experimental AOM parameters for tetrahedral $[CoX_4]^{2-}$ systems. Published data depends either on an additional constraint for the ratio of e_σ and e_π,[39] or is even chosen randomly.[88] Therefore review articles and book chapters listing the parameters have to be read with some caution.[27]

The fitting procedure outlined above was applied to the series of cobalt halide complexes. The e_σ and e_π parameters in Table 1 show the expected trend of $F^- > Cl^- > Br^- > I^-$ according to their donor capabilities and positioning in the spectrochemical series. The parameters fitted to the matrices based on the CASSCF and NEVPT2 data follow the same trend, but do show some numerical differences that are discussed in some more detail in the Supporting Information. A comparison with experimental and computational ligand field splitting values is also provided in the Supporting Information.

Having the e_σ and e_π parameters in hand, we calculated the ratio e_σ/e_π. This is the first time that this ratio has been calculated from individually obtained parameters, as opposed to requiring the parameters to meet a predefined ratio.[39,40] The values found, see Table 1, lie within the expected range for halide ligands in various complexes, ranging roughly from 2 to 5.[27] Most notably, the often assumed ratio of 4 for cobalt halide complexes is not reproduced here.

As a side note, the fitting procedure confirms the expectation of d–s mixing not being relevant: when fitting the systems with e_{ds}, the parameter restraints are hit and the parameter has no influence on the cost of the fit.

Table 1. AOM parameters for $[CoX_4]^{2-}$ in tetrahedral geometry. Each data point is the average of five calculations with the standard deviation given in parentheses.

Method	Complex	E [cm^{-1}]	e_σ [cm^{-1}]	e_π [cm^{-1}]	e_σ/e_π
CASSCF	$[CoF_4]^{2-}$	−1 211 563(52)	5432(26)	2298(20)	2.36(2)
	$[CoCl_4]^{2-}$	−1 224 735(19)	3146(10)	1101(9)	2.86(3)
	$[CoBr_4]^{2-}$	−1 229 806(54)	2662(27)	872(21)	3.05(8)
	$[CoI_4]^{2-}$	−1 237 432(44)	2090(22)	630(17)	3.32(10)
NEVPT2	$[CoF_4]^{2-}$	−1 213 192(71)	5274(36)	2225(27)	2.37(3)
	$[CoCl_4]^{2-}$	−1 226 664(41)	3150(21)	1118(16)	2.82(4)
	$[CoBr_4]^{2-}$	−1 231 835(86)	2717(44)	917(33)	2.96(12)
	$[CoI_4]^{2-}$	−1 239 611(111)	2216(56)	719(43)	3.08(20)

Dependence on the bond length

The ligand field splitting is a function of the metal-ligand distance r. Crystal field theory predicts that:[25,p. 38]

$$\Delta_{tet} = \frac{20ze^2\langle a^4\rangle}{27r^5}, \tag{10}$$

whereas taking the ligand as a dipole instead of a point charge would result in a distance dependence of r^{-6}.[25,p. 39] Here, ze^2 refers to the charge of a ligand and a d electron, and a to the radius of the d shell. While the relation was derived for octahedral symmetry, the only difference in tetrahedral symmetry is a factor of 4/9. Since there is no such simple equation for ligands with more complicated charge distributions, the equation was generalised in the form[40,89–91]

$$\Delta \propto r^{-n}, \tag{11}$$

with n as a fitting parameter and an undefined proportionality constant.

The fitting procedure described herein allows us to quantitatively evaluate the distance dependence of all AOM parameters. The variation of the ligand field splitting Δ across the series of homoleptic cobalt halide complexes and point charges is shown in Figure 5. Rodríguez and Moreno state that the parameters A and n in $10Dq = Ar^{-n}$ are not necessarily constant over a wide range of r. They assume that the description applies in an interval of ± 0.1 Å around a given r.[90]

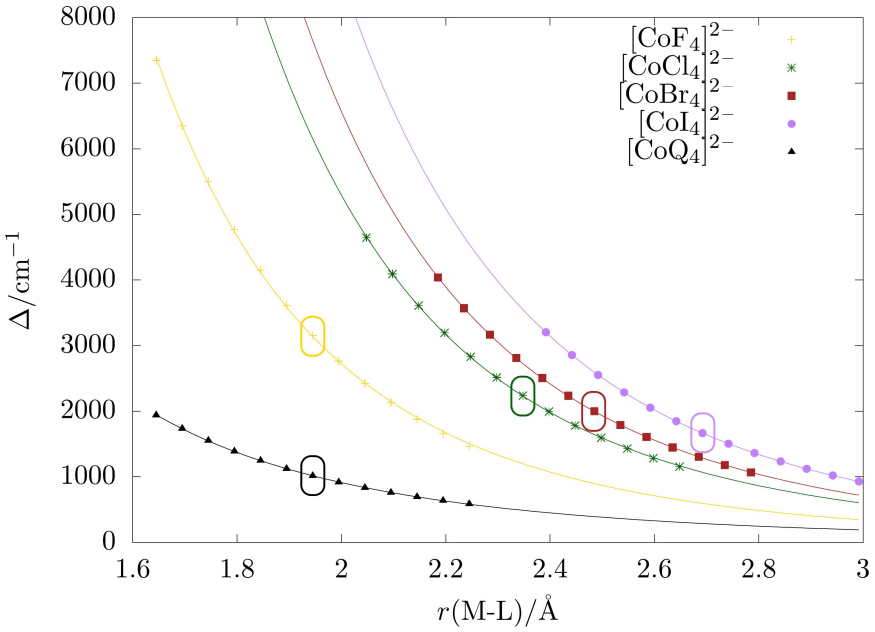

Figure 5. △ of homoleptic cobalt halides for different bond lengths, calculated with $\triangle = \varepsilon(t_2) - \varepsilon(e) = \frac{4}{3}e_\sigma - \frac{16}{9}e_\pi$. The respective equilibrium bond lengths are highlighted with boxes around the data points. Q denotes a point charge.

Our data shows that an excellent fit is obtained even with variations of ±0.2 Å around the equilibrium bond lengths. The exponent n increases from 5.12 in the fluoride complex to 5.53 in the iodide complex, in full agreement with the range determined experimentally. At first glance, this also fits to the assumption of an r^{-5} distance dependence for point charges and a r^{-6} relationship for dipoles: the hard fluoride ligand is usually seen as barely polarizable and therefore expected to act similar to a point charge. The softer and more polarizable the halide is, the more it is expected to act as a dipole. However, the aiLFT-AOM parameter fit for point charges at the positions of the fluoride ions in $[CoF_4]^{2-}$ yields an even lower value of $n = 3.83$. By this measure, fluoride thus appears to be much more polarizable than an actual point charge. Even though there are no immediately obvious practical implications of this knowledge, being able to quantitatively compare ligands in this way may be useful in other settings.

The proportionality constant A shows a trend too, with softer ligands yielding larger constants as show in Table 2. Since the charge of the ligands is constant, we put forward the interpretation that A corresponds to the d shell radius a in equation 10. The harder the ligand, the smaller is A and therefore the extent of the pure d orbitals in the ligand field picture.

Experimentally, different methods have been used to study the bond length dependence of Δ. It is calculated by measuring electronic transitions through UV-vis or photoluminescence spectroscopy. The bond length changes are achieved by compression experiments of crystals,[92–94] observations in different crystal lattices,[90,95] and comparisons of different ligands with the same donor atom.[96,97] Compression and lattice variation experiments have shown Δ dependencies of r^{-5} to r^{-6}. The third method depending on the donor atom is inherently flawed, because it mixes the effect of the bond length and of the different electronic properties of the ligands into the same interpretation; Bertini et al. call it "extremely simplified and rough".[96]

The fitting procedure introduced here allows us to separate electronic and structural effects and compute the distance dependence individually for the different AOM parameters. We studied the bond length dependence of AOM parameters for homoleptic and heteroleptic complexes. Because the situation is much more complicated for heteroleptic complexes, we focus on homoleptic ones below; additional data sets are shown in the Supporting Information.

Starting with the behaviour of E for different bond lengths r, see Figure 6, a first surprising observation is made: E decays as the bond length increases, but vastly different values for E are found at the same bond length for different halides. This finding might reflect variations in the spherical potential the central metal is subjected to and may be an effect of differences in the charge screening or charge distribution in the different halides.

The parameter e_σ decreases with increasing r with very little variation across the series of halide ligands, see Figure 6. This suggests that e_σ is only a function of r and independent of the

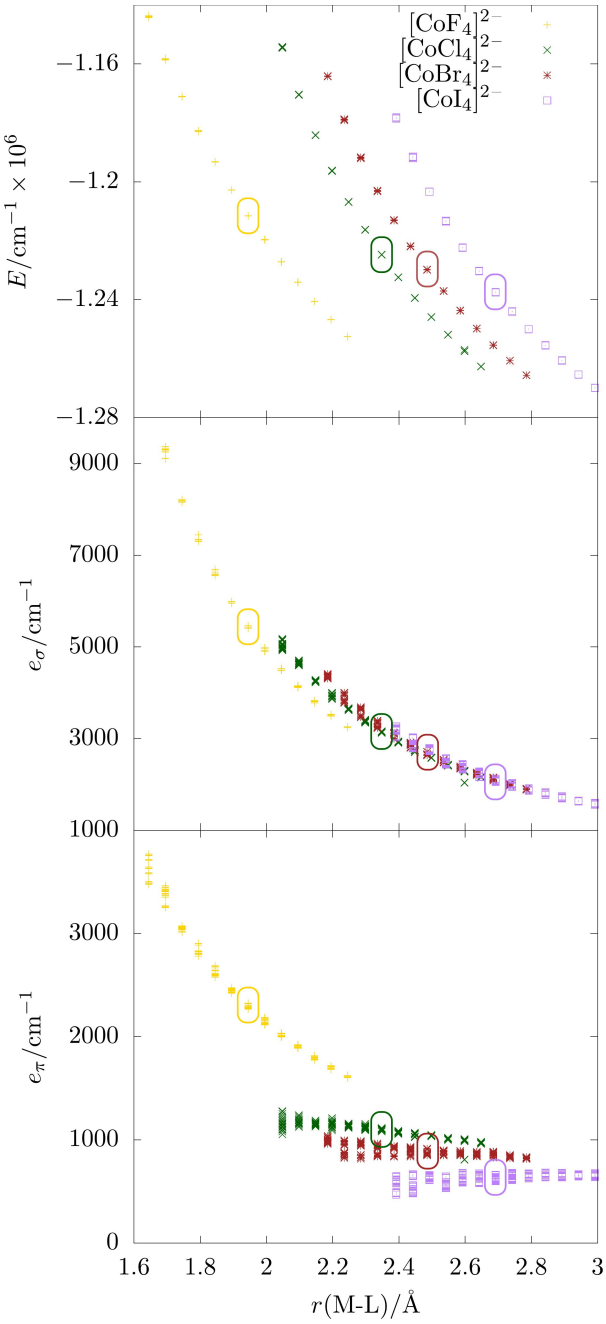

Figure 6. E, e_σ and e_π of homoleptic cobalt halides for different bond lengths. The respective equilibrium bond lengths are highlighted with boxes around the data points. Note that analogous plots are shown in the Supporting Information for Mn–Cu.

Table 2. Fitting parameters of $\triangle(r) = Ar^{-n}$ shown in Figure 5. Q denotes a point charge.

Complex	n	A
$[CoQ_4]^{2-}$	3.88	13402
$[CoF_4]^{2-}$	5.12	94482
$[CoCl_4]^{2-}$	5.39	221487
$[CoBr_4]^{2-}$	5.48	293771
$[CoI_4]^{2-}$	5.53	398624

halide element. The variation in e_π depends on the nature of the halide: for the heavier elements Cl, Br^- and I^-, e_π is almost constant. A plausible explanation might be that the increased σ-donation at shorter distances is compensated with reduced π-donation, thus ensuring electroneutrality. Therefore the π-interaction does not increase as may have been expected, but stays the same. For the lightest halide, F^-, e_π decays monotonically with increasing bond length. Fluoride is known to be much harder than the other halides and very often shows a unique chemical behaviour. Congruent with the above interpretation, fluoride appears less capable of ensuring electroneutrality, which we can trace back to its π-interaction with the central metal.

Transferability

Transferability of AOM parameters for the same ligand or ligand type between different complexes is an often assumed or expected feature, although it was also shown that it is not generally applicable.[42,64,96,98,99] It is usually applied to systems where the chemical environment of a certain M–L bond is seen as very similar.[20,42] For many heteroleptic complexes, the equation system will be underdetermined, precluding an individual fit for every AOM parameter. With the procedure presented herein, we are able to obtain $\mathbf{V}_{LF}$ with a high or complete degree of independent matrix elements. Our method can thus investigate heteroleptic complexes with highly symmetric equilibrium structures, which allows us to quantitatively evaluate the transferability of AOM parameters.

We investigated complexes of the type $[CoX_nY_{4-n}]^{2-}$, where *X* and *Y* are different halides. All *XY* combinations with the exception of $[CoF_3I_1]^{2-}$ are considered. Geometries are optimized without restraints and a bond length scan is performed. The results of the bond length scan are shown exemplarily for e_σ of the Co–Cl bond in Figure 7.

Despite the outliers occasionally found, there is a clear correlation between bond length and AOM parameter: shorter bond lengths lead to larger e_σ values. With regard to the stoichiometry, no clear trend can be observed. For F^-, e_σ decreases with an increasing portion of fluoride heteroligands. In the cases of bromide or iodide heteroligands, no such trend can be determined. Still, the heteroligand has an impact on the bond length of the subject ligand: soft halides tend to have longer bond lengths when another hard halide is present in the complex and vice versa.

To distinguish the effects of the M–X bond length and influence of the heteroligand, additional calculations were performed where each metal-ligand bond length in the complexes $[CoX_nY_{4-n}]^{2-}$ is fixed at the equilibrium bond length of the respective homoleptic complex. Accordingly, the M–X bonds are as long as the bonds in $[MX_4]^{2-}$ and the M–Y bonds have the same length as in $[MY_4]^{2-}$. The obtained AOM parameters refer to the Co–X bond. The results are shown in Table 3 and can be summarized for both e_σ and e_π as follows: the harder the ligand X, the less noticeable are possible trends; the harder the heteroligand Y, the smaller are the AOM

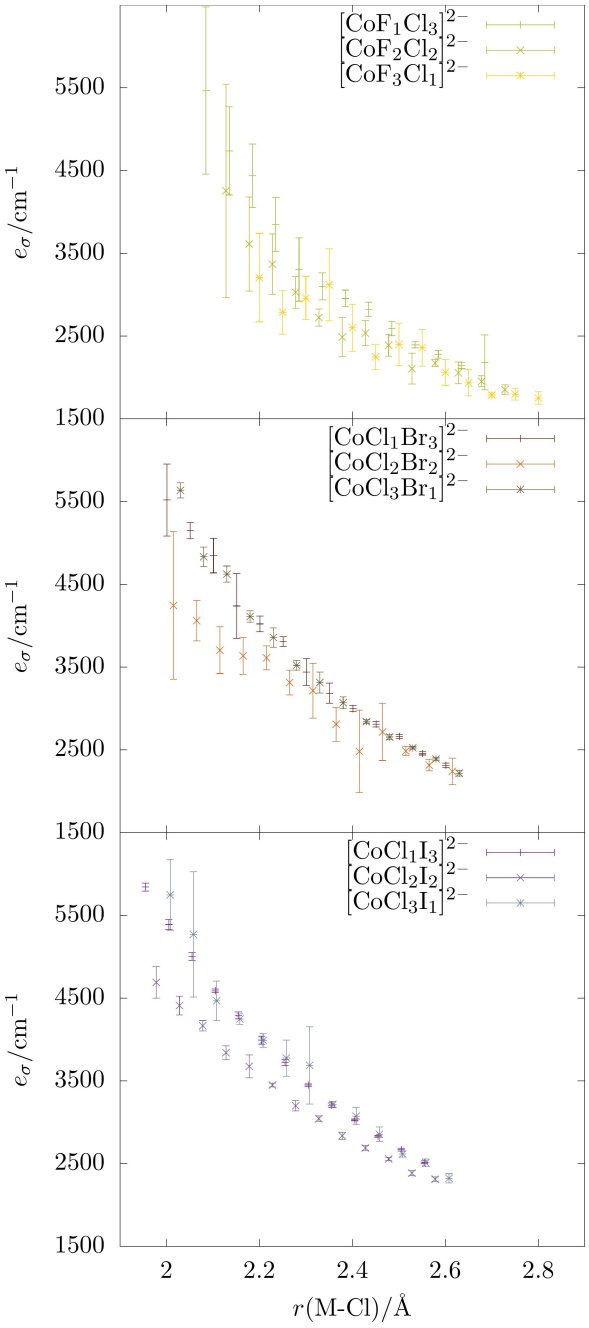

Figure 7. e_σ parameter of the Co–Cl bond in various complexes. Three outliers were removed, see Supporting Information for details.

parameters. Parameters for neighbouring Y are of similar size and almost never differ by more than 200 cm^{-1}.

Compared to the data of the optimized structures (see the Supporting Information) it seems that the influence of the heteroligand is mainly caused by the change in bond length. The obvious exception is fluoride, which has a significant impact at any bond length and every complex. This has two implications: many qualitative effects are already captured by the simple crystal field approach, in which only the charge or dipole moment at the ligands is relevant. On the other hand,

Table 3. AOM parameters for the Co–X bond in different complexes of the type $CoX_n Y_{4-n}$ with r(M–L) being the equilibrium bond length of the homoleptic complexes. The subject ligand X is printed in bold letters on the far left of the Table, n_X is its count in the respective complex. Y denotes the type of the hetero ligand, given in the second column. Parameters of homoleptic complexes with $n_X = 4$ are shown in italics for easier comparison. All numbers are the average of five data points with the standard deviation given in parentheses. Rows show the parameter change with the stoichiometry, with the homoleptic complex on the right. Columns show the parameter change in the same stoichiometry but with changing heteroligands; the entry for the homoleptic complex is the one where the heteroligand is the same as the subject ligand.

X	Y	e_σ/cm^{-1} n_X 1	2	3	4	e_π/cm^{-1} n_X 1	2	3	4
F	F	*5432(26)*	*5432(26)*	*5432(26)*	*5432(26)*	*2298(20)*	*2298(20)*	*2298(20)*	*2298(20)*
	Cl	5330(65)	5325(101)	5385(82)	*5432(26)*	2387(53)	2322(82)	2309(75)	*2298(20)*
	Br	5322(42)	5365(64)	5474(423)	*5432(26)*	2436(41)	2384(54)	2399(326)	*2298(20)*
	I	5372(150)	5352(162)	5178(151)	*5432(26)*	2538(112)	2418(123)	2208(115)	*2298(20)*
Cl	F	2997(92)	3045(101)	3116(67)	*3146(10)*	879(47)	946(83)	1027(56)	*1101(9)*
	Cl	*3146(10)*	*3146(10)*	*3146(10)*	*3146(10)*	*1101(9)*	*1101(9)*	*1101(9)*	*1101(9)*
	Br	3204(28)	3179(65)	3042(304)	*3146(10)*	1184(22)	1142(52)	1030(224)	*1101(9)*
	I	3227(55)	3089(117)	3216(52)	*3146(10)*	1281(55)	1131(92)	1186(53)	*1101(9)*
Br	F	2463(421)	2504(69)	2594(61)	*2662(27)*	565(306)	643(70)	763(58)	*872(21)*
	Cl	2469(288)	2610(63)	2635(27)	*2662(27)*	667(227)	793(49)	834(28)	*872(21)*
	Br	*2662(27)*	*2662(27)*	*2662(27)*	*2662(27)*	*872(21)*	*872(21)*	*872(21)*	*872(21)*
	I	2764(174)	2711(93)	2669(94)	*2662(27)*	1021(139)	953(81)	895(77)	*872(21)*
I	F	1427(151)	1869(186)	2086(193)	*2090(22)*	−45(91)	341(159)	558(155)	*630(17)*
	Cl	1956(64)	1848(110)	2047(32)	*2090(22)*	415(58)	361(77)	553(32)	*630(17)*
	Br	2015(99)	2075(103)	2107(160)	*2090(22)*	501(71)	561(83)	614(120)	*630(17)*
	I	*2090(22)*	*2090(22)*	*2090(22)*	*2090(22)*	*630(17)*	*630(17)*	*630(17)*	*630(17)*

the bond lengths change in real complexes, so while it would be valid to assume roughly the same $e_\lambda(r)$ for a certain M–L bond in different complexes, r will not be identical.

Summed up, transferability in the given systems is at least questionable. Because ligands have a significant influence on each others bond lengths and they mutually influence their interaction with the metal, their AOM parameters are likely to differ in different chemical settings. Having shown that the black-box fitting procedure presented herein facilitates not only the identification of an ideal AOM parameter set for a given system, but also the distance dependence of one or more ligands, it is now possible to evaluate the error made when transferring the AOM parameters of a particular ligand type between complexes. In any case, the parameters in a specific complex can be used to assess the electronic properties of a ligand in a certain environment in a qualitative and chemically understandable way.

Two-Dimensional Spectrochemical Series and Chemical Hardness

Having shown with a thorough investigation of $[CoX_4]^{2-}$ complexes and their heteroleptic variants that our fitting procedure provides reliable results that agree with experiment and offer various opportunities for chemical interpretation, we now discuss the two-dimensional spectrochemical series $[M^{II}X_4]^{2-}$ with M = Mn, Fe, Co, Ni, Cu, and X = F, Cl, Br, I. The metals form the Irving–Williams series, for which the observed 'double-bump' trend in the hydration enthalpies is explained with differences in their ligand field stabilisation energies.[100–102] While the d^7 configuration of Co^{2+} leads to perfectly tetrahedral structures that are straightforward to analyse and interpret, there are a few caveats for other members of the series. The Fe, Ni and Cu complexes are subject to Jahn–Teller distortion, the exact shape of which depends on the metals. For Fe, there is a slight change in bond angles, the Ni complexes have two shorter and two longer bond lengths, whereas the Cu complexes are "flattened" and have D_{2d} symmetry. Experimental references for these complexes are listed in the Supporting Information.

As shown in Table 4, the general trends for E, e_σ and e_π are the same even for the more asymmetric structures. Of note is the sensitivity of the method, which for instance discerns the different e_π parameters in the nickel halides as the metal-halide bond is varied, see graphs in the Supporting Information analogous to Figure 6. Overall, Table 4 shows that the AOM

Table 4. AOM parameters E, e_σ and e_π for homoleptic metal halides with the metals Mn, Fe, Co, Ni, Cu.

Complex	E/cm^{-1}	e_σ/cm^{-1}	e_π/cm^{-1}	e_σ/e_π
$[MnF_4]^{2-}$	−715 961(98)	5988(52)	2560(42)	2.34(4)
$[MnCl_4]^{2-}$	−734 463(64)	3422(33)	1258(27)	2.72(6)
$[MnBr_4]^{2-}$	−741 496(48)	2825(26)	982(27)	2.88(8)
$[MnI_4]^{2-}$	−749 106(25)	2265(16)	750(20)	3.02(8)
$[FeF_4]^{2-}$	−945 787(68)	6900(91)	2920(106)	2.36(9)
$[FeCl_4]^{2-}$	−966 124(81)	3427(35)	1252(28)	2.74(7)
$[FeBr_4]^{2-}$	−971 604(144)	2796(51)	943(44)	2.97(15)
$[FeI_4]^{2-}$	−979 423(273)	2151(27)	656(25)	3.28(13)
$[CoF_4]^{2-}$	−1 211 563(52)	5359(168)	2252(111)	2.38(14)
$[CoCl_4]^{2-}$	−1 224 735(19)	3146(10)	1101(9)	2.86(3)
$[CoBr_4]^{2-}$	−1 229 806(54)	2662(27)	872(21)	3.05(8)
$[CoI_4]^{2-}$	−1 237 432(44)	2043(135)	594(103)	3.44(64)
$[NiF_4]^{2-}$	−1 492 974(30)	5213(162)	2248(140)	2.32(16)
$[NiCl_4]^{2-}$	−1 503 065(45)	3128(98)	1144(95)	2.73(24)
$[NiBr_4]^{2-}$	−1 507 380(69)	2671(92)	920(101)	2.90(33)
$[NiI_4]^{2-}$	−1 513 307(61)	2121(84)	672(84)	3.16(41)
$[CuF_4]^{2-}$	−1 823 377(19)	5331(179)	2353(162)	2.27(17)
$[CuCl_4]^{2-}$	−1 835 433(26)	3035(51)	1124(48)	2.70(12)
$[CuBr_4]^{2-}$	−1 841 224(38)	2507(41)	876(31)	2.86(11)
$[CuI_4]^{2-}$	−1 847 959(14)	1930(36)	623(26)	3.10(14)

parameters are mainly influenced by the ligand, while the metal series show rather subtle differences. The only exception is $[FeF_4]^{2-}$ with notably larger e_σ and slightly larger e_π values than seen in the rest of the series. Compared with an earlier study based on Average-of-Configuration-KS-DFT, we find smaller e_σ values and e_σ/e_π ratios (e.g. for $[FeCl_4]^{2-}$: $e_\sigma = 0.471(4)$ μm^{-1}, $e_\sigma/e_\pi = 3.00$).[103] It will be interesting to study such a 2D-spectrochemical series for octahedral coordination environments, where the influence of the metal is expected to be much more pronounced for differential occupation of the σ–e_g and π–t_{2g} sets since the σ and π bonding modes are more cleanly separated than in tetrahedral systems.

Two-dimensional spectrochemical series separate and compare the σ and π contribution in a metal-ligand interaction.[104,105] The e_σ and e_π parameters obtained from our procedure are plotted against each other, see Figure 8, as is commonly done for such series.[22] The points show a linear relationship and can be fitted almost perfectly with a common regression line, pointing out again the above finding that the spectrochemical series for the metals is much less pronounced in the present cases than for the halides. Our data show that there is one equation that relates e_σ and e_π for all complexes investigated here. This finding can be used as a constraint that complements the relationship between Δ and the e-parameters ($\Delta = \varepsilon(t_2) - \varepsilon(e)$), and thus enables AOM parameter fits for perfectly tetrahedral $[MX_4]^{2-}$ complexes without information on the off-diagonal elements. In contrast to the approach using empirical ratios mentioned in the introduction (e.g. $e_\pi = 4e_\sigma$ for Cl^-[40]), this observation includes all halides. Studies on $[V^{III}X_4]^-$ and $[Cr^{IV}X_4]$,[106] $[M^{III}Cl_6]^{2-}$ with M = Cr, Mo, W, $[CrX_6]^{3-}$ with X = CN^-, NH_3, F^-, Cl^-, Br^-, I^-,[31] and Ni^{II} complexes[107] had found similar relationships for other ligand types and metal charges. Even though a direct comparison is not possible due to the different protocols used here and in the previous examples, the correlation lines for different ligand types but the same metal appear to lie parallel to each other.

In the previous sections, we often referred to chemical hardness in a qualitative way to rationalize and compare the effect of different ligands. In order to probe whether the concept can be applied quantitatively, the Pearson hardness of the halides is plotted against their AOM parameters in the homoleptic complexes at their equilibrium geometries in Figure 9.[60] The plots are essentially perfectly linear for the σ and π parameters, showing that the concept of chemical hardness is suitable to explain the observed effects. Since the AOM parameters are very similar for the different metals, the resulting regression lines lie close to each other; as mentioned above, $[FeF_4]^{2-}$ is an exception here. While for each metal series, a linear relationship between the hardness of the halide ligands and the AOM parameters is obtained, it will have to be evaluated whether this holds for other types of ligand. It cannot be expected that all ligands will fall on the same line, but series of ligands with similar donor capabilities may show a correlation within the series.

Conclusions

Ligand Field Theory and the Angular Overlap Model are powerful ideas that allow chemists to intuitively interpret the electronic structures of coordination complexes based on their building blocks. With the aiLFT analysis now readily available to translate complex quantum chemical wavefunctions into a ligand field picture,[50] chemists can study arbitrary coordination complexes in great detail from a ligand field perspective.[32,35,52–55] The AOM provides ligand-specific parame-

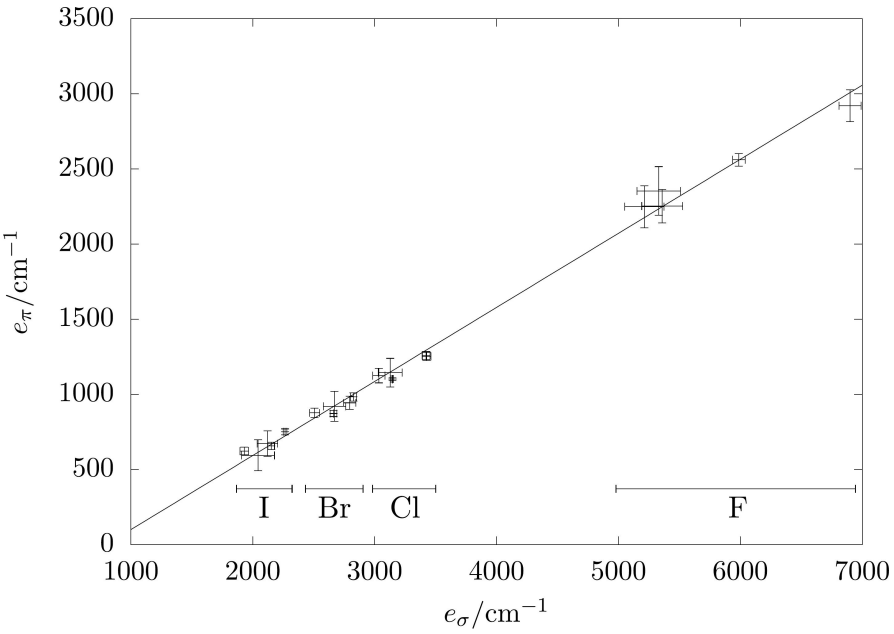

Figure 8. e_σ vs. e_π for different metal halides, all metals shown in the same color and fitted with a common regression line. Error bars indicate the standard deviation. The regression line is the function $e_\pi = 0.4929e_\sigma - 394$ cm^{-1}. Regression lines for the individual metal series are given in the Supporting Information.

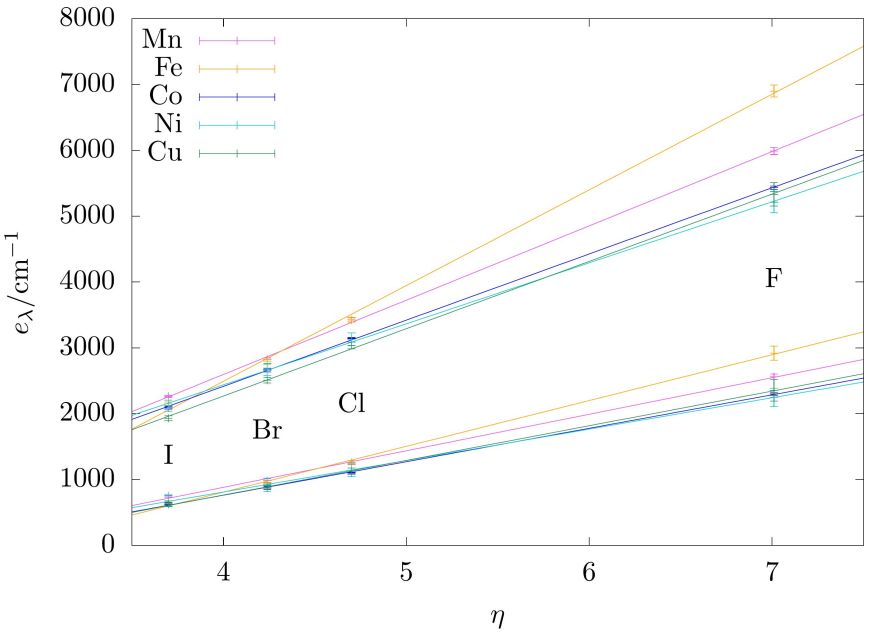

Figure 9. Calculated AOM parameters of various halido metalates versus the chemical hardness η of X with their respective linear regression lines. The hardness values are taken from [60].

ters, e_σ and e_π, that describe the individual ligand–metal interactions in terms of the widely used σ- and π-terminology. However, obtaining AOM parameters for such complexes previously required detailed knowledge of the underlying equation systems and significant experience in applying and solving them. Therefore, we have developed an automated fitting procedure for AOM parameters based on a scheme for generating asymmetric coordination environments with subsequent aiLFT analyses.

The protocol established here provides AOM parameters for any complex the model is applicable to, and is not limited by the availability or resolution of experimental data, that is, AOM parameters can even be generated for complexes where fits were not possible before. In addition, the procedure used herein naturally includes the spherical ligand field potential *E*, which was not considered in any of the fitting schemes previously reported in the literature. We are confident that having easy access to the AOM parameters e_σ, e_π and e_{ds} for any complex that falls under the remits of the AOM and aiLFT analyses, including any structural distortions or modifications that may be useful to answer a given chemical question, will help in better understanding their electronic structures and coordination chemistry.

With a series of tetrahedral cobalt halide complexes as a case study, we have shown that the numerical values found with our procedure are in agreement with experimental data and have standard deviations much below the uncertainties that were previously commonly accepted. We quantitatively evaluated how the bond length *r* affects the ligand field splitting Δ, the spherical ligand field potential *E* and the AOM parameters e_σ and e_π. The behaviour of fluoride differs from that of the heavier halides, which led us to conclude that it is much less capable of ensuring electroneutrality in these complexes. Given the often unusual behaviour of fluoride ligands, it will be interesting to verify this effect in other series of halide complexes, ideally in conjunction with spectroscopy methods that are sensitive to the charge distribution around the central metal.

Due to the limited number of independent matrix elements available for fitting, a commonly used practice is to transfer the AOM parameters found for a particular ligand type from one complex to another. We evaluated how sensitive the AOM parameters of the halide ligands are to the overall composition of the complex and showed that this practice is at least inaccurate. As a common rule, we deduced that in cases where the other ligands have high donor or acceptor capabilities compared to the ligand for which the parameters are to be transferred, AOM parameter transfer is prone to failure. The fitting procedure presented herein allows a detailed quantification of the errors made when AOM parameter transfer cannot be avoided, e.g. in cases where too few matrix elements are available for fitting.

Pearson's principle of hard and soft acids and bases relies on the chemical hardness, a quantity that is calculated as the average of a species' ionisation potential and electron affinity.[59,60] As such, it can in principle be measured with high accuracy, even though the HSAB concept is used rather intuitively in everyday chemistry arguments. We found a previously unknown linear relationship between the chemical hardness of the ligands and their AOM parameters for all series of metal complexes in the two-dimensional spectrochemical series from Mn–Cu. It will be interesting to explore whether this relationship holds for other types of ligand, which may provide an additional aspect to the comparison and quantification of

ligand character in coordination complexes. Within the two-dimensional spectrochemical series involving all halides of Mn–Cu, we found a common relationship between e_σ and e_π. This finding can act as an additional constraint in future fitting procedures. Comparison with similar series in the literature showed that other types of ligand fall on approximately parallel lines. The e_σ–e_π relationship can thus serve as a tool for characterising the metal-ligand interaction in a two-dimensional map, which might be particularly useful in the context of developing structure–property relationships.

The above examples illustrate a few avenues in which the AOM parameter fitting scheme can be used to better understand the ligand–metal interactions and cooperative effects in coordination complexes. Future work will involve more complex ligands, e.g. ligands in which e_{π_x} and e_{π_y} will be differentiated and multidentate ligands. With the capability of fitting AOM parameters in an unbiased and automated fashion, several other ideas can be studied quantitatively in future, e.g. d–s mixing (or coordination voids) and misdirected bonding effects, which have previously been accounted for by introducing new parameters. Since the procedure introduced here will allow us to avoid overparameterisation and quantify the uncertainty associated with each parameter, we will be able to carefully evaluate their physical and chemical meaning.

Going beyond the specific interpretations of individual AOM parameters, we are convinced that having access to an automated AOM parameter fitting scheme will make it much easier for chemists to interpret electronic structures or design desirable electronic structures by evaluating the effects of ligand substitution patterns and changes in coordination geometry through the AOM lens, whether these are specific design criteria for catalysis, molecular magnetism or other desirable ground state properties.

Acknowledgements

Calculations for this research were conducted on the Lichtenberg high performance computer of the TU Darmstadt. Open Access funding enabled and organized by Projekt DEAL.

Conflict of Interest

The authors declare no conflict of interest.

Data Availability Statement

The data that support the findings of this study are available from the corresponding author upon reasonable request.

Keywords: *ab initio* calculations · angular overlap model · ligand effects · ligand field theory · transition metal complexes

[1] D. J. Durand, N. Fey, *Chem. Rev.* **2019**, *119*, 6561–6594.
[2] F. Neese, *Coord. Chem. Rev.* **2009**, *253*, 526–563.
[3] F. Neese, T. Petrenko, D. Ganyushin, G. Olbrich, *Coord. Chem. Rev.* **2007**, *251*, 288–327.
[4] R. Francke, B. Schille, M. Roemelt, *Chem. Rev.* **2018**, *118*, 4631–4701.
[5] P. Comba, B. Martin in *Adv. Inorg. Chem. Vol. 73*, Elsevier, **2019**, pp. 305–322.
[6] C.-H. Wang, S. DeBeer, *Chem. Soc. Rev.* **2021**, *50*, 8743–8761.
[7] C. J. Ballhausen, H. B. Gray, *Inorg. Chem.* **1962**, *1*, 111–122.
[8] T. Helgaker, S. Coriani, P. Jørgensen, K. Kristensen, J. Olsen, K. Ruud, *Chem. Rev.* **2012**, *112*, 543–631.
[9] C. J. Cramer, D. G. Truhlar, *Phys. Chem. Chem. Phys.* **2009**, *11*, 10757–10816.
[10] L. González, D. Escudero, L. Serrano-Andrés, *ChemPhysChem* **2012**, *13*, 28–51.
[11] J. P. Malrieu, R. Caballol, C. J. Calzado, C. de Graaf, N. Guihéry, *Chem. Rev.* **2014**, *114*, 429–492.
[12] V. Krewald, M. Retegan, F. Neese, W. Lubitz, D. A. Pantazis, N. Cox, *Inorg. Chem.* **2016**, *55*, 488–501.
[13] M. Gerloch, *Magnetism and Ligand-Field Analysis*, Cambridge University Press, New York, **1983**.
[14] C. J. Ballhausen, *Introduction to ligand field theory*, McGraw-Hill, New York, **1962**.
[15] J. S. Griffith, L. E. Orgel, *Q. Rev. Chem. Soc.* **1957**, *11*, 381.
[16] L. E. Orgel, *J. Chem. Soc.* **1952**, 4756.
[17] W. H. Kleiner, *J. Chem. Phys.* **1952**, *20*, 1784–1791.
[18] C. E. Schäffer, *Inorg. Chim. Acta* **1995**, *240*, 581–592.
[19] C. E. Schäffer, H. Yamatera, *Inorg. Chem.* **1991**, *30*, 2840–2853.
[20] M. Gerloch, R. G. Woolley, *J. Chem. Soc. Dalton Trans.* **1981**, 1714.
[21] M. Gerloch, J. H. Harding, R. G. Woolley in *Inorganic Chemistry*, Springer, Berlin, **1981**, pp. 1–46.
[22] C. Anthon, J. Bendix, C. E. Schäffer, *Inorg. Chem.* **2004**, *43*, 7882–7886.
[23] R. Deeth in *Comprehensive Coordination Chemistry II*, Elsevier, **2003**, pp. 439–442.
[24] C. E. Schäffer, C. K. Jørgensen, *Mol. Phys.* **1965**, *9*, 401–412.
[25] B. N. Figgis, M. A. Hitchman, *Ligand Field Theory and Its Applications*, 1st ed., Wiley, New York, **2000**.
[26] C. E. Schäffer, *Pure Appl. Chem.* **1970**, *24*, 361–392.
[27] A. Bencini, C. Benelli, D. Gatteschi, *Coord. Chem. Rev.* **1984**, *60*, 131–169.
[28] E. C. Wasinger, F. M. F. de Groot, B. Hedman, K. O. Hodgson, E. I. Solomon, *J. Am. Chem. Soc.* **2003**, *125*, 12894–12906.
[29] M. Gerloch, R. G. Woolley in *Progress Inorganic Chemistry* Wiley, New York, **1984**, pp. 371–446.
[30] A. Ceulemans, M. Dendooven, L. G. Vanquickenborne, *Inorg. Chem.* **1985**, *24*, 1153–1158.
[31] S. K. Singh, J. Eng, M. Atanasov, F. Neese, *Coord. Chem. Rev.* **2017**, *344*, 2–25.
[32] D. Schweinfurth, M. G. Sommer, M. Atanasov, S. Demeshko, S. Hohloch, F. Meyer, F. Neese, B. Sarkar, *J. Am. Chem. Soc.* **2015**, *137*, 1993–2005.
[33] J. Jung, M. Atanasov, F. Neese, *Inorg. Chem.* **2017**, *56*, 8802–8816.
[34] G. Charron, F. Bellot, F. Cisnetti, G. Pelosi, J.-N. Rebilly, E. Rivière, A.-L. Barra, T. Mallah, C. Policar, *Chem. Eur. J.* **2007**, *13*, 2774–2782.
[35] J. Krzystek, D. C. Swenson, S. A. Zvyagin, D. Smirnov, A. Ozarowski, J. Telser, *J. Am. Chem. Soc.* **2010**, *132*, 5241–5253.
[36] A. Bronova, N. Kannengießer, R. Glaum, *Inorg. Chem.* **2017**, *56*, 9235–9246.
[37] N. Kannengießer, M. Jähnig, R. K. Kremer, R. Glaum, *Eur. J. Inorg. Chem.* **2021**, *2021*, 1722–1735.
[38] M. Suta, F. Cimpoesu, W. Urland, *Coord. Chem. Rev.* **2021**, *441*, 213981.
[39] D. A. Cruse, M. Gerloch, *J. Chem. Soc. Dalton Trans.* **1977**, 1617.
[40] R. Glaum, M. A. Hitchman, *Aust. J. Chem.* **1996**, *49*, 1221.
[41] R. G. Woolley, *Mol. Phys.* **1981**, *42*, 703–720.
[42] M. Gerloch in *Understanding Molecular Properties*, **1987**, pp. 111–142.
[43] R. J. Deeth, *Dalton Trans.* **2020**, *49*, 9641–9650.
[44] R. J. Deeth, *Eur. J. Inorg. Chem.* **2020**, *2020*, 1960–1963.
[45] M. Atanasov, C. Daul, H. U. Güdel, T. A. Wesolowski, M. Zbiri, *Inorg. Chem.* **2005**, *44*, 2954–2963.
[46] M. Atanasov, C. A. Daul, *C. R. Chim.* **2005**, *8*, 1421–1433.
[47] C. E. Schäffer, C. Anthon, J. Bendix, *Coord. Chem. Rev.* **2009**, *253*, 575–593.
[48] C. Daul, *Chimia* **2014**, *68*, 633–641.
[49] F. Vlahović, M. Perić, M. Gruden-Pavlović, M. Zlatar, *J. Chem. Phys.* **2015**, *142*, 214111.

[50] M. Atanasov, D. Ganyushin, K. Sivalingam, F. Neese in *Molecular Electronic Structures of Transition Metal Complexes II, Structure and Bonding* **2011**, pp. 149–220.
[51] L. Lang, M. Atanasov, F. Neese, *J. Phys. Chem. A* **2020**, *124*, 1025–1037.
[52] E. A. Suturina, D. Maganas, E. Bill, M. Atanasov, F. Neese, *Inorg. Chem.* **2015**, *54*, 9948–9961.
[53] Y. Rechkemmer, F. D. Breitgoff, M. van der Meer, M. Atanasov, M. Hakl, M. Orlita, P. Neugebauer, F. Neese, B. Sarkar, J. van Slageren, *Nat. Commun.* **2016**, *7*, 10467.
[54] M. A. Palacios, I. F. Díaz-Ortega, H. Nojiri, E. A. Suturina, M. Ozerov, J. Krzystek, E. Colacio, *Inorg. Chem. Front.* **2020**, *7*, 4611–4630.
[55] S. E. Stavretis, M. Atanasov, A. A. Podlesnyak, S. C. Hunter, F. Neese, Z.-L. Xue, *Inorg. Chem.* **2015**, *54*, 9790–9801.
[56] M. Atanasov, D. Aravena, E. Suturina, E. Bill, D. Maganas, F. Neese, *Coord. Chem. Rev.* **2015**, *289–290*, 177–214.
[57] V. Lyaskovskyy, B. de Bruin, *ACS Catal.* **2012**, *2*, 270–279.
[58] O. R. Luca, R. H. Crabtree, *Chem. Soc. Rev.* **2013**, *42*, 1440–1459.
[59] R. G. Pearson, *J. Am. Chem. Soc.* **1963**, *85*, 3533–3539.
[60] R. G. Pearson, *J. Am. Chem. Soc.* **1988**, *110*, 7684–7690.
[61] F. Neese, *Wiley Interdiscip. Rev.: Comput. Mol. Sci.* **2012**, *2*, 73–78.
[62] V. G. Chilkuri, S. DeBeer, F. Neese, *Inorg. Chem.* **2017**, *56*, 10418–10436.
[63] R. J. Deeth, D. L. Foulis, *Phys. Chem. Chem. Phys.* **2002**, *4*, 4292–4297.
[64] R. G. Woolley, *Int. Rev. Phys. Chem.* **1987**, *6*, 93–141.
[65] R. J. Deeth, A. Anastasi, C. Diedrich, K. Randell, *Coord. Chem. Rev.* **2009**, *253*, 795–816.
[66] W. H. Press, *Numerical Recipes: The Art of Scientific Computing*, 3rd ed., Cambridge University Press, Cambridge, **2007**.
[67] F. Neese, *WIREs Comput. Mol. Sci.* **2018**, *8*, e1327.
[68] A. D. Becke, *Phys. Rev. A* **1988**, *38*, 3098–3100.
[69] J. P. Perdew, *Phys. Rev. B* **1986**, *33*, 8822–8824.
[70] F. Weigend, R. Ahlrichs, *Phys. Chem. Chem. Phys.* **2005**, *7*, 3297.
[71] P. Siegbahn, A. Heiberg, B. Roos, B. Levy, *Phys. Scr.* **1980**, *21*, 323–327.
[72] B. O. Roos, P. R. Taylor, P. E. Siegbahn, *Chem. Phys.* **1980**, *48*, 157–173.
[73] C. Angeli, R. Cimiraglia, J.-P. Malrieu, *Chem. Phys. Lett.* **2001**, *350*, 297–305.
[74] C. Angeli, R. Cimiraglia, S. Evangelisti, T. Leininger, J.-P. Malrieu, *J. Chem. Phys.* **2001**, *114*, 10252–10264.
[75] C. Angeli, R. Cimiraglia, J.-P. Malrieu, *J. Chem. Phys.* **2002**, *117*, 9138–9153.
[76] C. Angeli, R. Cimiraglia, *Theor. Chem. Acc.* **2002**, *107*, 313–317.
[77] N. M. Barrera, J. L. McCarty, V. Dragojlovic, *Chem. Educ.* **2002**, *7*, 142–145.
[78] S. Buffagni, T. M. Dunn, *Nature* **1960**, *188*, 937–938.
[79] N. Fogel, C. C. Lin, C. Ford, W. Grindstaff, *Inorg. Chem.* **1964**, *3*, 720–726.
[80] K. Kojima, J. Matsuda, *Bull. Chem. Soc. Jpn.* **1986**, *59*, 859–863.
[81] M. R. Pressprich, R. D. Willett, *Acta Crystallogr. Sect. C Cryst. Struct. Commun.* **1991**, *47*, 1188–1191.
[82] Y. Nishihata, A. Sawada, H. Kasatani, H. Terauchi, *Acta Crystallogr. Sect. C Cryst. Struct. Commun.* **1993**, *49*, 1939–1941.
[83] V. V. Sharutin, V. S. Senchurin, O. K. Sharutina, O. A. Fastovets, A. P. Pakusina, *Russ. J. Inorg. Chem.* **2010**, *55*, 1410–1414.
[84] V. V. Sharutin, V. S. Senchurin, O. K. Sharutina, B. B. Kunkurdonova, *Russ. J. Inorg. Chem.* **2011**, *56*, 1384–1389.
[85] W. Klemm, W. Brandt, R. Hoppe, *Z. Anorg. Allg. Chem.* **1961**, *308*, 179–189.
[86] J. V. Rau, N. S. Chilingarov, L. N. Sidorov, *Rapid Commun. Mass Spectrom.* **1997**, *11*, 1977–1979.
[87] M. I. Nikitin, A. S. Alikhanyan, *Russ. J. Inorg. Chem.* **2020**, *65*, 199–204.
[88] W. D. Horrocks, D. A. Burlone, *J. Am. Chem. Soc.* **1976**, *98*, 6512–6516.
[89] M. Bermejo, L. Pueyo, *J. Chem. Phys.* **1983**, *78*, 854–857.
[90] F. Rodríguez, M. Moreno, *J. Chem. Phys.* **1986**, *84*, 692–697.
[91] P. V. Bernhardt, P. Comba, *Inorg. Chem.* **1993**, *32*, 2798–2803.
[92] H. G. Drickamer, *J. Chem. Phys.* **1967**, *47*, 1880.
[93] D. W. Smith, *J. Chem. Phys.* **1969**, *50*, 2784.
[94] D. R. Stephens, H. G. Drickamer, *J. Chem. Phys.* **1961**, *35*, 427–429.
[95] M. C. M. de Lucas, F. Rodríguez, H. U. Güdel, N. Furer, *J. Lumin.* **1994**, *60–61*, 581–584.
[96] I. Bertini, D. Gatteschi, A. Scozzafava, *Inorg. Chem.* **1976**, *15*, 203–207.
[97] A. B. P. Lever, I. M. Walker, P. J. McCarthy, K. B. Mertes, A. Jircitano, R. Sheldon, *Inorg. Chem.* **1983**, *22*, 2252–2258.
[98] M. Gerloch, R. F. McMeeking, A. M. White, *J. Chem. Soc. Dalton Trans.* **1976**, 655–660.
[99] R. J. Deeth, M. Gerloch, *Inorg. Chem.* **1985**, *24*, 1754–1758.
[100] D. A. Johnson, P. G. Nelson, *Inorg. Chem.* **1995**, *34*, 3253–3259.
[101] D. A. Johnson, P. G. Nelson, *J. Chem. Soc. Dalton Trans.* **1995**, 3483–3488.
[102] R. J. Deeth, K. Randell, *Inorg. Chem.* **2008**, *47*, 7377–7388.
[103] C. E. Schäffer, C. Anthon, J. Bendix, *Aust. J. Chem.* **2009**, *62*, 1271.
[104] D. S. McClure in *Solid State Physics*, (Eds.: D. Turnbull, H. Ehrenreich), Elsevier, Burlington, **1959**, pp. 399–525.
[105] W. W. Fee, J. N. Harrowfield, *Aust. J. Chem.* **1970**, *23*, 1049.
[106] C. Anthon, J. Bendix, C. E. Schäffer in *Optical Spectra and Chemical Bonding in Transition Metal Complexes* (Ed.: T. Schönherr), Springer, Berlin, **2004**, pp. 207–301.
[107] M. Atanasov, P. Comba, S. Helmle, D. Müller, F. Neese, *Inorg. Chem.* **2012**, *51*, 12324–12335.

Manuscript received: October 19, 2021
Accepted manuscript online: January 3, 2022
Version of record online: February 2, 2022